Nanoscale

Cite this: *Nanoscale*, 2012, **4**, 1776

www.rsc.org/nanoscale

PAPER

Honeycomb architecture of carbon quantum dots: a new efficient substrate to support gold for stronger SERS†

Yueqiong Fan,[a] Huhu Cheng,[a] Ce Zhou,[a] Xuejun Xie,[a] Yong Liu,[b] Liming Dai,[bc] Jing Zhang[a] and Liangti Qu*[a]

Received 17th December 2011, Accepted 9th January 2012
DOI: 10.1039/c2nr12015a

The rational assembly of quantum dots (QDs) in a geometrically well-defined fashion opens up the possibility of accessing the full potential of the material and allows new functions of the assembled QDs to be achieved. In this work, well-confined two-dimensional (2D) and 3D carbon quantum dot (CQD) honeycomb structures have been assembled by electrodeposition of oxygen-rich functional CQDs within the interstitial voids of assemblies of SiO_2 nanospheres, followed by extraction of the SiO_2 cores with HF treatment. Although made from quantum sized carbon dots, the CQD assemblies present a solid porous framework, which can be further used as a sacrificial template for the fabrication of new nanostructures made from other functional materials. Based on the unique honeycomb architecture of the CQDs, which allows the more efficient adsorption of molecules, the formed Au nanoparticles on the CQD honeycomb exhibit 8–11 times stronger surface enhanced Raman scattering (SERS) effect than the widely used Au nanoparticle SERS substrate for the highly sensitive detection of target molecules. This work provides a new approach for the design and fabrication of ultrasensitive SERS platforms for various applications.

Introduction

Monodisperse nanodots or nanocrystals have presented a wide range of novel phenomena at the nanoscale that are distinct from those of the bulk materials.[1–3] Their unique applications in electronic, magnetic and optical devices have attracted intense attention.[4] However, some of the promising potential of these materials in applications such as field-effect transistors,[5–7] light-emitting devices,[8] photodetectors,[9] photoconductors,[10] and solar cells[11] are directly related to the densely packed ensembles of nanodots with multidimensionally ordered hierarchical architectures. As a consequence, the current scope of nanoscience is moving forward from the fundamental synthesis of building blocks to the study of the collective properties of nanodot ensembles and their hierarchical architectures.[12–14] There is a broad range of examples of nanocrystal self-organization into highly periodic two- (2D) and three-dimensional (3D) ordered sturctures.[2,15] Well-confined assemblies offer the opportunity to control the collective functions associated with magnetic, optical and electronic coupling between the individual nanodots. As such, development of the method which governs the controlled assembly of these well-defined structures is of scientific and industrial interest and is significant in creating new and high-performance tunable materials with unique functions.[16–19]

Carbon quantum dots[20,21] (CQDs) have attracted a great deal of attention in recent years due to their promise in bioimaging,[22–25] optoelectronic devices,[26,27] pollutant detection[28] and catalysis.[29,30] Compared with conventional inorganic quantum dots, CQDs have many advantages, including low toxicity, chemical inertness and biocompatibility. In particular, their high resistance to photobleaching makes them attractive materials for optoelectronics[31] and *in vivo* biosensing applications.[32,33] In addition, typical CQDs contain a large amount of carboxylic and hydroxyl groups at their surfaces, thus endowing them with excellent water solubility and the suitability for subsequent functionalization with various organic, polymeric, inorganic or biological species. It is well acknowledged that environmentally benign CQDs with well-defined dimensions, tunable surface functionalities and a simple, fast and cheap synthetic route provide encouraging building blocks for the construction of advanced functional architectures. However, to date, there have been no reports on the rational assembly of CQDs into functional configurations, and hence their collective properties remain unknown.

Herein, we present one example where CQDs are used as the basic building block for the controllable construction of macroscopic honeycomb structures *via* the assistance of a pre-assembled 2D or 3D silica colloid template. The resultant CQD

[a]*Key Laboratory of Cluster Science, Ministry of Education, School of Chemistry, Beijing Institute of Technology, Beijing, 100081, China. E-mail: lqu@bit.edu.cn; Fax: +86 10 68918608; Tel: +86 10 68918608*
[b]*Institute of Advanced Materials for Nano-Bio Applications, School of Ophthalmology and Optometry, Wenzhou Medical College, Wenzhou, Zhejiang, 325027, China*
[c]*Department of Macromolecular Science and Engineering, Case School of Engineering, Case Western Reserve University, 10900 Euclid Avenue, Cleveland, Ohio, 44106, United States*
† Electronic supplementary information (ESI) available. See DOI: 10.1039/c2nr12015a

honeycombs can not only be used as a sacrificial template for the fabrication of new nanostructures made from other functional materials, but also provide a new platform for the fabrication of a more efficient SERS substrate than the widely used Au nanofilm.

Experimental

Preparation of CQDs

CQDs were prepared by an electrochemical method similar to our previous report.[26] A graphite rod with a size of *ca.* 3.0 cm × 0.5 cm was used as a working electrode. Pt wire and Ag/AgCl were used as counter and reference electrodes, respectively. The electrolyte was 0.1 M phosphate buffer solution (PBS) at pH 7.0. With the use of a CHI660D electrochemical workstation, a cyclic voltammetric (CV) scan within the potential region of ±3.0 V at a scan rate of 0.1 V s^{-1} was applied for the preparation of CQDs. After the electrochemical reaction was complete, the water soluble CQDs were collected by filtration of the resulting solution through a 20 nm filter membrane, followed by dialysis of the aqueous solution with a cellulose ester membrane bag (MD77 (8000-14000)) for several days. After fully removing the supporting electrolyte (PBS), the purified CQDs were re-dispersed in deionized water for further use.

Preparation of 2D and 3D CQD honeycomb structures

First, a monolayer of SiO_2 nanospheres (200 nm in diameter) was self-assembled onto a conductive N-doped Si substrate (5 mm by 5 mm) by following the previously reported procedure.[34] The formation of 3D colloidal crystals was accomplished by evaporation-induced multilayer assembly. These Si supported SiO_2 nanosphere assemblies were used as the anode for electrophoretic deposition of CQDs in the aqueous CQD suspension with a concentration of *ca.* 0.04 mg mL^{-1} under a voltage of 5 V for 3 h and 12 h for 2D and 3D CQD honeycomb structures, respectively. The CQDs infiltrated the SiO_2 nanosphere assemblies and were then annealed at 600 °C for 1 h under an argon flow. Finally, SiO_2 cores were removed by dilute HF acid (10%) treatment, followed by rinsing with deionized water. 2D and 3D CQD honeycomb structures were obtained after drying at room temperature. X-Ray photoelectron spectroscopy (XPS) analysis was utilized to verify the removal of SiO_2 nanospheres (Fig. S1†).

Preparation of Au honeycomb structures

The as-formed CQD honeycomb was used as the sacrificial template for the preparation of Au honeycomb structures. Au was deposited on the CQD honeycomb by direct sputter coating of a *ca.* 40 nm Au layer under a vacuum of 1.2 Pa and a sputtering current of 6 mA. Then, the CQDs were fully removed by heat at *ca.* 450 °C in air for 1 h.

Characterization

The morphologies of the samples were examined by scanning (SEM, JEOL) and transmission (TEM, JEM-2010) electron microscopy. TEM observations were performed with lacey support films coating the TEM grid and operating at 200 kV. The elemental analyses of the samples were deduced by X-ray energy dispersive spectroscopy (EDS, equipped on the SEM). Fourier transform infra-red (FT-IR) spectra were recorded on a Bruker spectrometer (Equinox 55/S) using KBr pellets. X-Ray photoelectron spectroscopy (XPS) data were obtained with an ESCALab220i-XL electron spectrometer from VG Scientific using 300 W Al Kα radiation. The base pressure was about 3×10^{-9} mbar. The binding energies were referenced to the C 1s line at 284.8 eV from adventitious carbon.

To investigate the SERS effect, *ca.* 15 nm thick Au was simultaneously sputtered onto the Si and CQD assembled honeycomb structures under the same conditions. Rhodamine 6G (R6G) molecules were adsorbed on the Au-coated and Au-free CQD honeycombs or on a Au nanoparticle film by simply soaking them in the aqueous solution of 4×10^{-6} M R6G. The soaking time was 1 h and the free molecules were removed by a stream of N_2 gas. One droplet of the corresponding R6G solution was also dropped on to the Si substrate and used as a reference for the Raman characterizations after drying. The Raman spectra were measured under ambient conditions using a Renishaw MicroRaman spectroscopy system with a 632.8 nm HeNe laser. The laser beam was focused by a 50× (NA = 0.75) objective lens resulting in a spot size of around 2 μm in diameter. The laser power on the samples was *ca.* 4.7 mW and the acquisition time was 30 s for the collection of each spectrum.

Results and discussion

The electrochemical preparation of CQDs was performed in 0.1 M PBS. The as-prepared CQD solution was found to exhibit a long-term homogeneous phase without any noticeable precipitation at room temperature (Fig. 1a). The TEM image shows the collected CQDs are fairly monodisperse and have a uniform size of *ca.* 3–6 nm (Fig. 1b), which is similar to electrochemically synthesized graphene-based nanodots.[26,35] The high resolution TEM image reveals a layer-by-layer structure with a *ca.* 0.35 nm spacing, consistent with the graphite interlayer distance. XPS measurements were performed to probe the composition of the

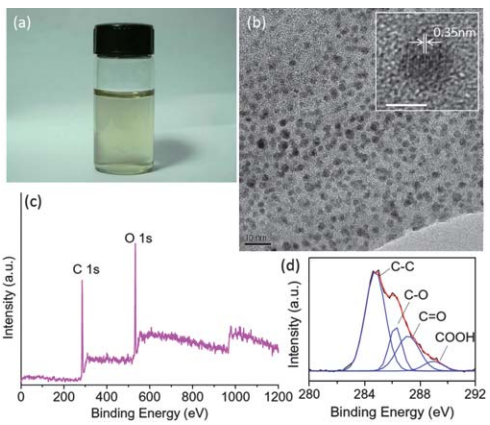

Fig. 1 A photo of functional CQDs dispersed in water (a), a TEM image of the as-prepared CQDs (b), the XPS spectrum of the CQDs (c) and the corresponding high resolution spectra of the C 1s peak (d). The scale bar in (b) is 10 nm. The inset in (b) is a high magnification image of a CQD and the scale bar is 5 nm.

as-produced CQDs. As can be seen in Fig. 1c, the XPS survey shows a predominant graphitic C 1s peak at *ca.* 284 eV and an O 1s peak at *ca.* 532 eV. The O/C atomic ratio is *ca.* 40%, which indicates an enrichment of the oxygen-related functional groups along the CQDs. The high resolution spectrum of C 1s (Fig. 1d) revealed the presence of C–C (284.8 eV), C–O (286.8 eV), C═O (287.8 eV) and COOH (289 eV) bonds,[26,36] indicating the as-prepared CQDs are rich in hydroxyl, carbonyl and carboxylic acid groups on their surfaces. Consistent with the XPS results, the FT-IR spectrum presented strong bands centered at *ca.* 3500 cm^{-1} and 1650 cm^{-1}, confirming the existence of hydroxyl and carbonyl groups once more.

The as-prepared CQDs are rich in negatively-charged carboxyl groups, thus imparting them with excellent water solubility and providing the opportunity for direct electrophoresis deposition for the formation of template-dependent complex structures. A schematic illustration of the preparation procedure adopted to form 2D CQD honeycombs is shown in Fig. 2. First, a single layer of monodisperse colloidal SiO_2 nanospheres was assembled on the flat conductive silicon wafer (Fig. 2a and b) using the so-called Langmuir–Blodgett (LB)-like technique,[34] which then serves as a template for the electrodeposition of CQDs under an applied voltage of 5 V (Fig. 2c). The relatively high electric field provides the driving force for the CQDs' motion and deposition despite a concomitant electrostatic repulsion being present. The formed core/shell structure of the CQDs enwrapping the SiO_2 nanospheres was annealed at 600 °C for 1 h to reinforce the binding among the CQDs (Fig. 2d). Finally, the SiO_2 cores were removed by dilute HF etching and the CQD honeycomb was thus obtained (Fig. 2e).

As shown in Fig. 3a and b, a large area of the CQD honeycomb structure can be formed on a Si substrate by virtue of the assembled SiO_2 nanosphere template (Fig. 2). The top views (Fig. 3a and b) show the circular micropores, which are consistent with the size of the SiO_2 microspheres. The tilted top views of the sample further verify the honeycomb microporous structure and clearly show the open mouths of the honeycomb (Fig. 3c and d). The almost transparent honeycomb structures are observed in Fig. 3d, which shows that the walls formed by the CQDs are quite thin.

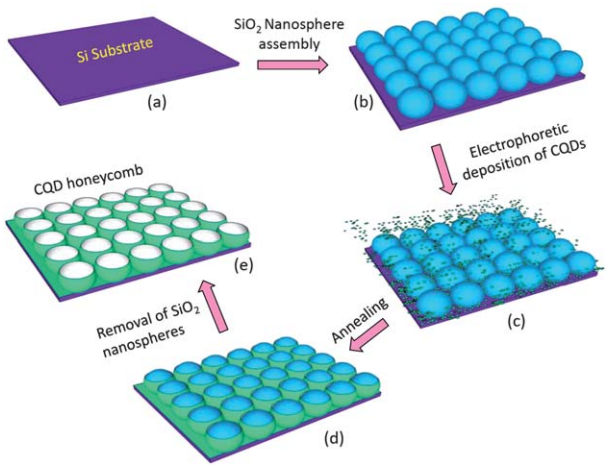

Fig. 2 A scheme of the fabrication process for the formation of a 2D honeycomb structure of CQDs.

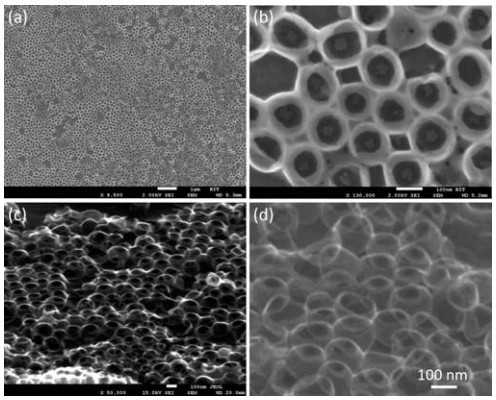

Fig. 3 Top (a, b) and tilted (c, d) SEM images of the as-prepared CQD honeycomb structures with different magnifications. Scale bars: a = 1 μm, and b–d = 100 nm.

The 3D honeycomb structures of the CQDs can also be obtained by use of a 3D colloidal nanosphere template (Fig. 4a). In this case, the multi-layer stacking of SiO_2 nanospheres was first formed on the conductive Si substrate, followed by electrodeposition of functional CQDs under similar conditions to those used in the formation of the 2D CQD honeycomb structure mentioned above. The low-magnification SEM image shown in Fig. 4b clearly shows the 3D structure at the fracture section of the formed honeycomb. The top views displayed in Fig. 4c and d reveal that the honeycomb morphology is similar to that shown in Fig. 3a and b. The side view (Fig. 4e and f) shows the run-through porosity and multi-layer stacking of the CQD hollow structure, which replicates the size of the SiO_2 nanospheres. As

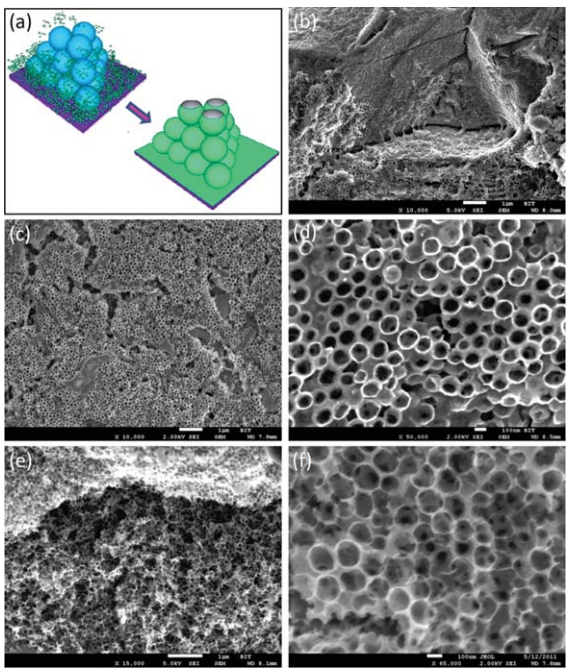

Fig. 4 3D CQD honeycomb structures. (a) A scheme of the fabrication process for the 3D CQD honeycomb structure, (b) a fracture region, (c–f) top and side views of the 3D CQD honeycomb structure with different magnifications. Scale bars: b, c and e are 1 μm; d and f are 100 nm.

a matter of fact, both the pore size and the wall thickness of the formed CQD honeycomb can be simply controlled by adjusting the size of the SiO_2 nanospheres and the deposition duration.

Fig. 5 shows the TEM images of the 2D and 3D assembled honeycomb structures of the CQDs. The walls of the CQD honeycomb are *ca.* 10 nm thick and, thus, are transparent under electron irradiation, which is consistent with the SEM observations shown in Fig. 3d. The area-selected electron diffraction pattern of the honeycomb wall shows bright rings with spots, indicating that the CQDs within the honeycomb structure still remain crystalline in nature after electrodeposition.

The formed CQD honeycomb can also be used as a sacrificial template to fabricate nanostructures composed of other materials. As demonstrated in Fig. 6a and b, we have prepared a Au honeycomb structure by simply sputtering Au on the CQD assembly. By doing so, the CQD honeycomb was fully covered with a Au film. Then, the CQDs were fully removed by heating at *ca.* 450 °C in air for a certain time. The thickness of the deposited Au layer is *ca.* 40 nm in the current case. The formed Au honeycomb has a relatively smaller mouth than that of the original CQD counterpart, but the honeycomb structure remains intact after the thermal treatment to remove the CQDs. Energy-dispersive X-ray spectroscopy (EDS) (Fig. 6c) clearly shows a dominant Au peak, accompanied by Si from the substrate and a small O peak, which is probably due to physical adsorption of oxygen or other contaminants. The C peak is negligibly low. These results indicate that the CQDs have been almost completely removed during the thermal treatment and the Au honeycomb can be formed without significant deformation.

Au nanoparticles have been widely used as efficient enhancers for Raman scattering and this phenomenon is known as the surface-enhanced Raman scattering (SERS) effect.[37] This enhancement effect is believed to be due to the excitation of the surface plasmon resonance (SPR) on the metal surface, which greatly strengthens the local *E*-field near the surface. Important applications of SERS can be found in chemistry, biology and material science as an ultra-sensitive detection technique capable of identifying trace molecules.[38–40] Conventional SERS substrates are constructed by placing metal nanoparticles on planar surfaces, which thereby have a limited surface area. The replacement of these planar surfaces by spatially-defined nanoporous surfaces with large surface areas will absorb more molecules for SERS signals and further improve the Raman detection sensitivity. Indeed, Jiang and coworkers[41] have demonstrated that the Raman enhancement effect can be dramatically improved by replacing the planar surface with a unique nanoporous super-aligned carbon nanotube film with cross stacking.

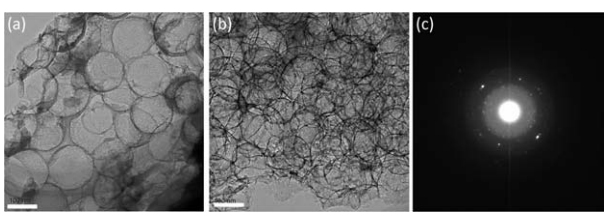

Fig. 5 TEM images of the CQD honeycomb structures in a 2D (a) and 3D (b) assembled fashion, and a typical electron diffraction pattern (c). Scale bars in a and b are 100 nm.

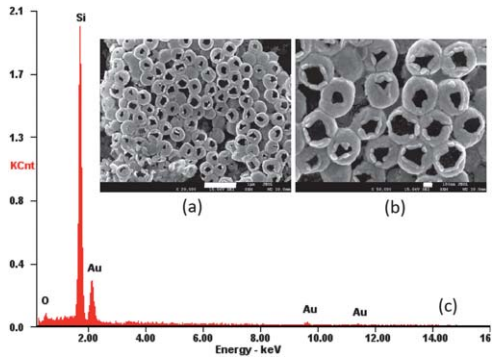

Fig. 6 SEM images of the as-prepared Au honeycomb structure with different magnifications (a, b), and the corresponding EDS spectrum (c). Scale bars: a = 1 μm and b = 100 nm.

Based on the hierarchical porous structure of the assembled CQD honeycombs, we also expect that the deposition of Au nanoparticles on the CQD honeycombs could achieve further enhanced Raman signals, which are better than that of the conventional SERS substrates. The SERS substrates were prepared by sputtering Au nanoparticles on to CQD honeycombs and flat Si surfaces under the same conditions. After Au deposition, the Au nanoparticles, with a size of *ca.* 15–25 nm, were formed on the Si surface (Fig. 7a). However, the deposited Au nanoparticles were spatially distributed on the walls of CQD

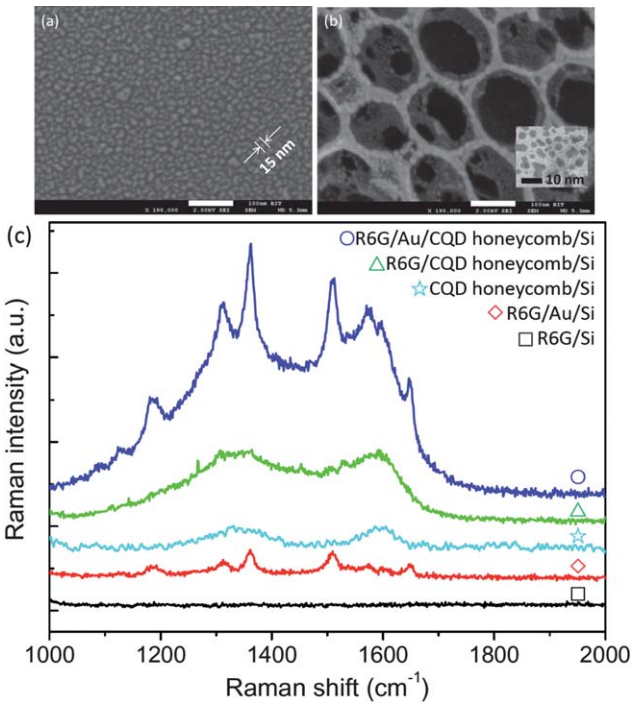

Fig. 7 SEM images of Au deposited on Si (a) and on the CQD honeycomb structure (b), and (c) the Raman spectra of 4×10^{-6} M R6G drop-cast on to a Si wafer (□), absorbed on Au coated Si (◇), the CQD honeycomb on Si (△), the Au-deposited CQD honeycomb on Si (○) and the Raman spectrum of the CQD honeycomb on Si (☆). The inset in (b) is a TEM image of the Au nanoparticles deposited on the wall of the CQD honeycomb. Scale bars in a and b are 100 nm.

honeycomb skeleton, and have a tiny size of less than of 10 nm (Fig. 7b). Except for the exposed edges, the observed small size of the Au nanoparticles on the walls of CQD honeycomb, in comparison with the size of the particles on the Si surface, is mainly attributed to the accessible large surface areas of the CQD honeycomb for Au nanoparticle deposition, which effectively avoids the accumulation and aggregation of Au nanoparticles.

To test the Raman enhancing capabilities of the honeycomb structure, an aqueous solution of Rhodamine 6G (R6G) (4×10^{-6} M) was applied to the SERS substrates. As shown in Fig. 7c, highly enhanced Raman peaks can be observed for R6G adsorbed on the Au-deposited CQD honeycomb, and the peak positions are similar to the previous reports,[42–44] while very weak Raman peaks for R6G can be observed on the pure CQD honeycomb. We also compared the Raman enhancement of the Au-deposited CQD honeycomb with a planar SERS substrate prepared by depositing Au onto a Si wafer under the same conditions. The Au-deposited CQD honeycomb substrate provides a much higher SERS signal than the Au/Si wafer, although the Au/Si substrate has already presented a strong SERS effect compared with a common Si wafer. Taking the Raman signal of R6G on the Au/Si SERS substrate as the reference, the Raman enhancement factor (EF) for the Au-deposited CQD honeycomb was estimated to be *ca.* 8–11 (Table 1). These results indicate that the Au-deposited CQD honeycomb is a more efficient SERS substrate than the widely used planar Au SERS substrate. Since the pure CQD honeycomb only shows typical carbon-related Raman peaks, and no Raman peaks associated to R6G were observed on the flat Si substrate, the observed Raman peaks of R6G, although very weak, on the CQD honeycomb structure indicate that the CQD assembly plays an essential role in enriching the R6G molecules for Raman scattering. On the other hand, the small Au particle size (<10 nm) and fairly uniform distribution along the CQD assembly may also further improve the Raman response.[41]

Conclusions

We have demonstrated the well-confined 2D and 3D assembly of CQDs into honeycomb frameworks by the simple electrodeposition of functional CQDs within pre-formed SiO_2 nanosphere templates. The assembly of the CQDs presents a hierarchical porous structure and can be further used as a sacrificial template for the fabrication of new nanostructures formed from other functional materials. Based on the unique honeycomb architecture of the CQDs, with a more efficient adsorption of molecules, the Au nanoparticles deposited on the CQD honeycombs exhibit an 8–11 times stronger SERS effect than the widely used Au nanoparticle SERS substrate for the highly sensitive detection of molecules. This work provides a new approach for the design and fabrication of ultra-sensitive SERS platforms for various applications.

Table 1 The calculated SERS EF for the different R6G bands based on the Au/Si substrate

Band position (cm^{-1})	EF
1648	8.2
1509	8.1
1360	8.8
1311	10.8
1185	7.9

Acknowledgements

This work was supported by the NSFC (21004006, 21174019 and 51161120361), NCET-10-0047, the Ministry of Science and Technology of China (2009DFB30380), the Zhejiang Department of Science and Technology (2009C13019) and the Ministry of Education (IRT1077).

Notes and references

1 C. Burda, X. B. Chen, R. Narayanan and M. A. El-Sayed, *Chem. Rev.*, 2005, **105**, 1025–1102.
2 C. B. Murray, C. R. Kagan and M. G. Bawendi, *Annu. Rev. Mater. Sci.*, 2000, **30**, 545–610.
3 D. L. Leslie-Pelecky and R. D. Rieke, *Chem. Mater.*, 1996, **8**, 1770–1783.
4 D. V. Talapin, J. S. Lee, M. V. Kovalenko and E. V. Shevchenko, *Chem. Rev.*, 2010, **110**, 389–458.
5 D. V. Talapin and C. B. Murray, *Science*, 2005, **310**, 86–89.
6 M. V. Kovalenko, M. Scheele and D. V. Talapin, *Science*, 2009, **324**, 1417–1420.
7 D. Yu, C. J. Wang and P. Guyot-Sionnest, *Science*, 2003, **300**, 1277–1280.
8 J. M. Caruge, J. E. Halpert, V. Wood, V. Bulovic and M. G. Bawendi, *Nat. Photonics*, 2008, **2**, 247–250.
9 G. Konstantatos, I. Howard, A. Fischer, S. Hoogland, J. Clifford, E. Klem, L. Levina and E. H. Sargent, *Nature*, 2006, **442**, 180–183.
10 H. Nakanishi, K. J. M. Bishop, B. Kowalczyk, A. Nitzan, E. A. Weiss, K. V. Tretiakov, M. M. Apodaca, R. Klajn, J. F. Stoddart and B. A. Grzybowski, *Nature*, 2009, **460**, 371–375.
11 I. Gur, N. A. Fromer, M. L. Geier and A. P. Alivisatos, *Science*, 2005, **310**, 462–465.
12 Z. H. Nie, A. Petukhova and E. Kumacheva, *Nat. Nanotechnol.*, 2010, **5**, 15–25.
13 C. L. Choi and A. P. Alivisatos, *Annu. Rev. Phys. Chem.*, 2010, **61**, 369–389.
14 P. Podsiadlo, B. Lee, V. B. Prakapenka, G. V. Krylova, R. D. Schaller, A. Demortiere and E. V. Shevchenko, *Nano Lett.*, 2011, **11**, 579–588.
15 C. B. Murray, C. R. Kagan and M. G. Bawendi, *Science*, 1995, **270**, 1335–1338.
16 T. Kashiwagi, F. Du, J. F. Douglas, K. I. Winey, R. H. Harris and J. R. Shields, *Nat. Mater.*, 2005, **4**, 928–933.
17 R. Shenhar, T. B. Norsten and V. M. Rotello, *Adv. Mater.*, 2005, **17**, 657–669.
18 S. Park, J. H. Lim, S. W. Chung and C. A. Mirkin, *Science*, 2004, **303**, 348–351.
19 R. K. Mallavajula and L. A. Archer, *Angew. Chem., Int. Ed.*, 2011, **50**, 578–580.
20 L. Y. Zheng, Y. W. Chi, Y. Q. Dong, J. P. Lin and B. B. Wang, *J. Am. Chem. Soc.*, 2009, **131**, 4564–4565.
21 Y. Dong, N. Zhou, X. Lin, J. Lin, Y. W. Chi and G. Chen, *Chem. Mater.*, 2010, **22**, 5895–5899.
22 L. Cao, X. Wang, M. J. Meziani, F. Lu, H. Wang, P. G. Luo, Y. Lin, B. A. Harruff, L. M. Veca, D. Murray, S. Y. Xie and Y. P. Sun, *J. Am. Chem. Soc.*, 2007, **129**, 11318–11319.
23 S. C. Ray, A. Saha, N. R. Jana and R. Sarkar, *J. Phys. Chem. C*, 2009, **113**, 18546–18551.
24 R. Liu, D. Wu, S. Liu, K. Koynov, W. Knoll and Q. Li, *Angew. Chem., Int. Ed.*, 2009, **48**, 4598.
25 S. Zhu, J. Zhang, C. Qiao, S. Tang, Y. Li, W. Yuan, B. Li, L. Tian, F. Liu, R. Hu, H. Gao, H. Wei, H. Zhang, H. Sun and B. Yang, *Chem. Commun.*, 2011, **47**, 6858–6860.
26 Y. Li, Y. Hu, Y. Zhao, G. Q. Shi, L. E. Deng, Y. B. Hou and L. T. Qu, *Adv. Mater.*, 2011, **23**, 776.

27 F. Wang, Y. Chen, C. Liu and D. Ma, *Chem. Commun.*, 2011, **47**, 3502–3504.
28 H. X. Zhan, L. Q. Liu, Z. D. Liu, Y. Wang, X. J. Zhao and C. Z. Huang, *Chem. Commun.*, 2011, **47**, 2604–2606.
29 L. Cao, S. Sahu, P. Anikumar, C. E. Bunker, J. Xu, K. A. S. Fernanodo, P. Wang, E. A. Guliants, K. N. Tackett and Y. P. Sun, *J. Am. Chem. Soc.*, 2011, **133**, 4754–4757.
30 H. Li, X. He, Z. Kang, H. Huang, Y. Liu, J. Liu, S. Lian, C. H. A. Tsang, X. Yang and S. T. Lee, *Angew. Chem., Int. Ed.*, 2010, **49**, 4430–4434.
31 X. Wang, L. Cao, F. S. Lu, M. J. Meziani, H. Li, G. Qi, B. Zhou, B. A. Harruff, F. Kermarrec and Y. P. Sun, *Chem. Commun.*, 2009, **25**, 3774–3776.
32 A. P. Alivisatos, W. Gu and C. Larabell, *Annu. Rev. Biomed. Eng.*, 2005, **7**, 55–76.
33 S. T. Yang, L. Cao, P. G. Luo, F. S. Lu, X. H. Wang, F. Wang, M. J. Meziani, Y. F. Liu, G. Qi and Y. P. Sun, *J. Am. Chem. Soc.*, 2009, **131**, 11308–11309.
34 M. Marquez and B. P. Grady, *Langmuir*, 2004, **20**, 10998–11004.
35 Y. Li, Y. Zhao, H. H. Cheng, Y. Hu, G. Q. Shi, L. M. Dai and L. T. Qu, *J. Am. Chem. Soc.*, 2012, **134**, 15–18.
36 J. Lu, J. X. Yang, J. Z. Wang, A. Lim, S. Wang and K. P. Loh, *ACS Nano*, 2009, **3**, 2367–2375.
37 P. L. Stiles, J. A. Dieringer, N. C. Shah and R. R. Van Duyne, *Annu. Rev. Anal. Chem.*, 2008, **1**, 601–626.
38 L. Gunnarsson, E. J. Bjerneld, H. Xu, S. Petronis, B. Kasemo and M. Käll, *Appl. Phys. Lett.*, 2001, **78**, 802–804.
39 G. L. Liu and L. P. Lee, *Appl. Phys. Lett.*, 2005, **87**, 074101.
40 H. H. Wang, C. Y. Liu, S. B. Wu, N. W. Liu, C. Y. Peng, T. H. Chan, C. F. Hsu, J. K. Wang and Y. L. Wang, *Adv. Mater.*, 2005, **17**, 222–225.
41 Y. Sun, K. Liu, J. Miao, Z. Wang, B. Tian, L. Zhang, Q. Li, S. Fan and K. Jiang, *Nano Lett.*, 2010, **10**, 1747–1753.
42 S. M. Nie and S. R. Emory, *Science*, 1997, **275**, 1102–1106.
43 A. M. Michaels, M. Nirmal and L. E. Brus, *J. Am. Chem. Soc.*, 1999, **121**, 9932–9939.
44 Y. Lu, G. L. Liu and L. P. Lee, *Nano Lett.*, 2005, **5**, 5–9.